Comparative analysis of GaN HEMT vs. Si CoolMOS for a High-Frequency MMC Topology

Ander Avila*, Asier Garcia-Bediaga*, Oier Oñederra°, Alejandro Rujas*, Alberto Rodriguez•

* IK4-IKERLAN Tech. Research Centre
Power Electronics Area
20500 Arrasate-Mondragón, Spain
aavila@ikerlan.es
http://www.ikerlan.es

° University of the Basque Country (UPV/EHU)
Electronics Technology Department
48013 Bilbao, Spain
oier.onederra@ehu.eus
https://www.ehu.eus

• Universidad de Oviedo
Grupo de Sistemas Electrónicos de Alimentación (SEA)
33204 Gijón, Spain
rodriguezalberto@uniovi.es
http://www.uniovi.es

Acknowledgments

This work was supported by the Project PowerBase. This project has received funding from the Electronic Component Systems for European Leadership Joint Undertaking under grant agreement No 662133. This Joint Undertaking receives support from the European Union's Horizon 2020 Research and Innovation Programme and Austria, Belgium, Germany, Italy, Netherlands, Norway, Slovakia, Spain and United Kingdom. This work was also supported by the Basque Government under the Emaitek Plus program and from the Government of Spain through project DPI2014-56358-JIN.

Keywords

≪Multilevel converters≫, ≪Gallium Nitride (GaN)≫, ≪Super junction devices≫

Abstract

The performance of a Modular Multilevel Converter (MMC) is presented in this paper, comparing Silicon (Si) and Gallium Nitride (GaN) semiconductors. Moreover, the benefits of high-frequency operation in a MMC topology are analysed along with a power loss distribution evaluation, highlighting the main advantages and drawbacks of different semiconductor technologies.

Introduction

Power switching devices based on Silicon (Si) have dominated the market of Switching Mode Power Supplies (SMPS) in the last decades. The main reasons are a good balance between performance and cost and a high reliability and maturity of the Si technology. However, the limits in terms of power density, temperature operation, and switching frequency of Si power devices are close to be reached [1]. The rapid evolution of power electronics tends to develop higher efficiency and higher power density SMPS. Great contributions of these goals are being carried out thanks to advanced power converter topologies, as well as new power semiconductor devices with better static and dynamic features [2].

From the point of view of power devices, the interest of industry and academia in Wide Band Gap (WBG) semiconductors has considerable increased in the last decade, especially for high-performance converters or in applications with strict requirements. In these terms, Silicon Carbide (SiC) and Gallium Nitride (GaN) are the most promising materials because of their beneficial properties and current availability [2]. Large energy gap and better electric field characteristics result in higher breakdown voltage capability for a thinner material. Consequently, the on-state resistance ($R_{DS_{on}}$) can be reduced, achieving lower conduction losses. While Si presents higher electron mobility, GaN and SiC can achieve high-switching operation as a result of high-saturation velocity.

Regarding advanced power converter topologies, Modular Multilevel Converter (MMC, M2C or M^2C) has gained attention, especially in the area of high-voltage direct current (HVDC) converters [3], Flexible AC Transmission Systems (FACTS) [4], and medium voltage drives (MVD) [5]. This topology was introduced in 2003 by Lesnicar and Marquardt [6], and it combines multilevel concept with modular structure by the use of cascaded sub-modules (SM) or cells, allowing the use of low voltage blocking devices.

Considering the use of WBG devices in MMC topology, SiC transistors have already been tested, achieving better performance than with Si devices [7], but there is no design or prototype with GaN devices up to date. Commercial GaN devices have relatively low blocking voltages (650V up to date) making difficult the use of these devices on medium/high voltage applications. However, thanks to the use of multilevel topologies, such as MMC, GaN devices can be used in applications where higher blocking voltages are required. Although GaN material benefits are already well known [2], it is not clear yet the benefits of current available GaN devices on medium/high power applications.

The main goal of this paper is to evaluate the performance of GaN High Electron Mobility Transistor (HEMT) in comparison with Si Super Junction devices (SJ), also known as CoolMOS, on a MMC topology. The operation frequencies of the MMC are analysed, highlighting the limitations and advantages of high-frequency operation. Furthermore, an analysis of power losses is performed, comparing GaN and Si power devices, together with an experimental validation of a GaN-based MMC cell.

Characteristics of devices under comparison

In spite of GaN material benefits, GaN devices characteristics do not clearly overcome its Si counterparts, mainly due to GaN power semiconductors early development stage. The main characteristics of GaN and Si devices with similar current and voltage maximum ratings are compared in Table I. For this comparison a low inductance package Si device is selected, as it will be analysed at high-frequency operation. These devices present similar $R_{DS_{on}}$ and output capacitance (C_{oss}) characteristic, being the main difference related to total gate charge (Q_G) and reverse recovery charge (Q_{rr}). GaN HEMT presents less gate charge than Si CoolMOS and negligible Q_{rr}. These distinctive features lead to high-switching and/or high-efficiency compactness solution.

Table I: Characteristics of devices under comparison.

Parameter		Si CoolMOS	GaN HEMT	Unit
Drain-to-source voltage	V_{DS}	650	650	[V]
Drain-to-source current	I_{DS}	29	30	[A]
On-state resistance *(T_j = 150 °C)*	$R_{DS_{on}}$	**125**	130	[mΩ]
Internal gate resistance	R_G	**0.8**	1.1	[Ω]
Total gate charge	Q_G	68	**5.8**	[nC]
Output capacitance	C_{oss}	54	65	[pF]
Recovery charge	Q_{rr}	6	**0**	[μC]
Gate pull-up resistance	$R_{g_{on}}$	10	10	[Ω]
Gate pull-down resistance	$R_{g_{off}}$	0	0	[Ω]
Gate driver turn-on voltage	$V_{GS_{on}}$	10	6.5	[V]
Gate driver turn-off voltage	$V_{GS_{off}}$	0	0	[V]
Gate driver voltage	$V_{plateau}$	5	3	[V]
Rise time	t_{ri}	5	**3.7**	[ns]
Fall time	t_{fi}	**3.5**	5.2	[ns]
Thermal resistance	$R_{th_{jc}}$	0.5	0.5	[K/W]

In order to compare the power losses produced by each device, conduction, switching, and driving losses are taken into account. On the one hand, driving losses can be estimated with (1).

$$E_{Driving} = \Delta V \cdot Q_G \qquad \text{where} \quad \Delta V = V = V_{GS_{on}} - V_{GS_{off}} \tag{1}$$

GaN HEMT presents lower ΔV and Q_G than Si CoolMOS, resulting in 18 times less gate driving energy for GaN HEMT. This feature results in high-switching operation, achieving low gate driver losses.

On the other hand, conduction and switching losses are obtained by the use of data-sheet parameters, outlined in Table I, along with an estimation of analytical commutation times proposed in [8, 9]. This application note is defined to estimate Si MOSFET power looses. In this case it is used for GaN HEMT and Si CoolMOS as their commutation performance is similar to Si MOSFET. Conduction losses can be estimated from the $R_{DS_{on}}$ characteristic, which depends on the junction temperature (T_j). Furthermore, turn-on switching energy (E_{on}) is obtained with (2). E_{on} characteristics are calculated taking into account the full energy of the reverse recovery process ($E_{on_{rr}}$) (3).

$$E_{on} = E_{on_i} + E_{on_{rr}} \tag{2}$$

$$E_{on_{rr}} = (Q_{rr} \cdot V_{DD}) \cdot (I_{D,on}/I_{rr})^{0.6} \cdot (V_{in}/V_{rr})^{0.6} \tag{3}$$

where V_{in} is the input voltage, $I_{D,on}$ is the switching current, and I_{rr} and V_{rr} are the reverse recovery current and voltage, respectively. Gate-to-drain capacitances (C_{GD1} and C_{GD2}) are obtained from the capacitances curves for different voltages as (4) defines.

$$E_{on_i} = V_{in} \cdot I_{D,on} \cdot \frac{t_{ri} + t_{fu}}{2} \qquad t_{fu} = (t_{fu1} + t_{fu2})/2 \qquad where \begin{cases} t_{fu1} = (V_{in} - R_{DS_{on}} \cdot I_{D,on}) \cdot C_{GD1}/I_{G,on} & \rightarrow C_{GD1} = C_{rss}(V_{DD}) \\ t_{fu2} = (V_{in} - R_{DS_{on}} \cdot I_{D,on}) \cdot C_{GD2}/I_{G,on} & \rightarrow C_{GD2} = C_{rss}(R_{DS_{on}} \cdot I_{D,on}) \\ I_{G,on} = (V_{GS_{on}} - V_{plateau})/(R_G + R_{g_{on}}) \end{cases} \tag{4}$$

The turn-off switching energy (E_{off}) can be estimated similarly using (5). In this case, the gate current ($I_{G,off}$) depends on the pull-down resistance (R_{goff}).

$$E_{off} = V_{in} \cdot I_{D,_{off}} \cdot \frac{t_{ru} + t_{fi}}{2} \qquad t_{ru} = (t_{ru1} + t_{ru2})/2 \qquad where \begin{cases} t_{ru1} = (V_{in} - R_{DS_{on}} \cdot I_{D,off}) \cdot C_{GD1}/I_{G,off} & \rightarrow C_{GD1} = C_{rss}(V_{DD}) \\ t_{ru2} = (V_{in} - R_{DS_{on}} \cdot I_{D,off}) \cdot C_{GD2}/I_{G,off} & \rightarrow C_{GD2} = C_{rss}(R_{DS_{on}} \cdot I_{D,off}) \\ I_{G_{off}} = (V_{GS_{off}} - V_{plateau})/(R_G + R_{g_{off}}) \end{cases} \tag{5}$$

Loss characteristics of both devices are estimated using these equations. Fig. 1(a) shows that CoolMOS has better conduction characteristic for a junction temperature (T_j) of 150 °C. Moreover, Si CoolMOS presents lower E_{off} than the GaN transistor (see Fig. 1(b)), being interesting for converters with soft-switching operation capability. However, it has to be noted that $E_{on_{rr}}$ is negligible in GaN devices. This characteristic is specially interesting for converters with hard-switching operation (such as MMC). On the contrary, $E_{on_{rr}}$ is the most influential factor for Si CoolMOS (2.7 mJ / $I_{D_{on}}$ = 20 A), making a difference between GaN and Si turn-on feature, as it is shown in Fig. 1(c).

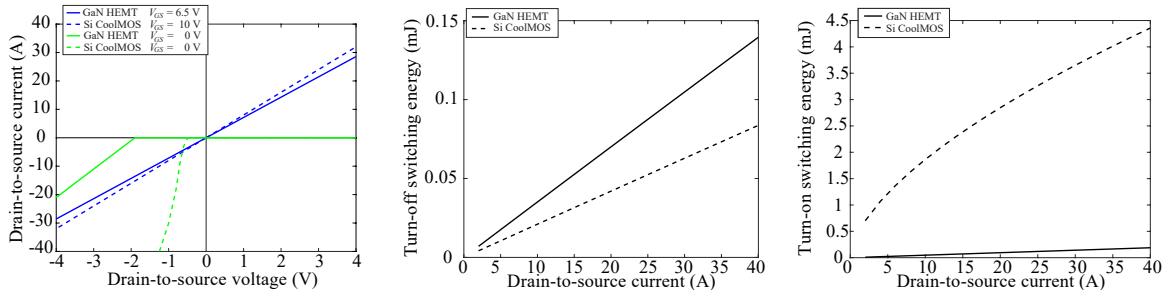

Fig. 1: GaN HEMT and Si CoolMOS devices characteristics comparison (V_{DD} = 400 V/ T_j = 150 °C): (a) Direct, reverse and open state conduction, (b) Turn-off switching energy (E_{off}) and (c) Turn-on switching energy (E_{on}).

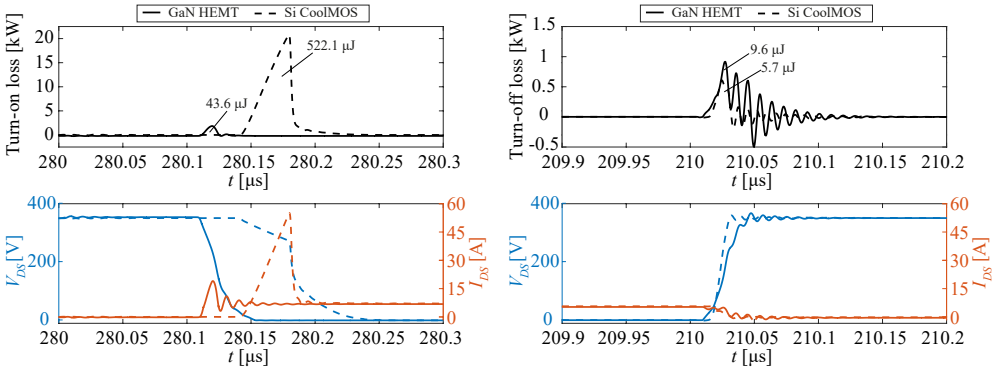

(a) (b)

Fig. 2: GaN HEMT and Si CoolMOS switching characteristics comparison by LTSPICE (V_{in} = 350 V/ T_j = 150 °C / I_{out} = 5A): Drain-to-source voltage (V_{DS}) and current (I_{DS}) together with switching and turn-on power losses (a) and turn-off power losses (b).

The switching performance of both technologies is also compared using SPICE models of these devices. The simulation is performed for a MMC half-bridge cell working in continuous conduction mode (CCM). The device based on GaN technology presents lower turn-on energy, due to the lower reverse recovery current as it is shown in Fig. 2(a). However, the turn-off performance of both devices is similar, achieving almost the same turn-off switching times (see Fig. 2(b)). Hence, in spite Si CoolMOS presents 12% less conduction losses than GaN devices and almost the same turn-off switching losses, there is a great difference in terms of turn-on switching losses.

MMC in high-frequency operation

With the aim of taking advantage of these high-frequency devices in high-power applications, this paper proposes the use of the MMC topology. The main advantages of MMC topology in medium and high-voltage applications are: its scalability, modularity and redundancy due to the series connection of cell; the possibility to operate without output filters or transformers and its good dynamic characteristics thanks to the increase of the switching frequency [10]. The impact of the modification of fundamental and switching frequency is analysed on a three-phase medium-voltage drive (MVD) (see Fig. 3 and Table II). In this converter, fundamental and switching frequency can be changed, depending on design criteria and operation point.

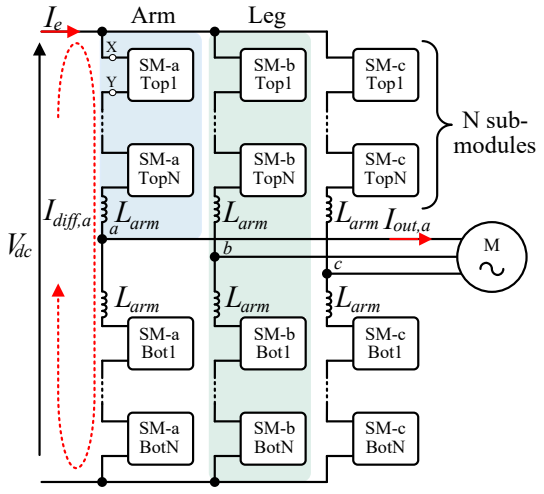

Fig. 3: Scaled three-phase MVD proposed for the frequency analysis.

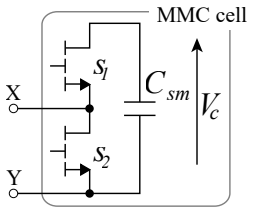

Fig. 4: GaN-based MMC SM.

Table II: Scaled MVD prototype specifications.

Parameter	Value	Unit
Input HVDC voltage V_{dc}	700	[V]
Output ac phase RMS voltage V_{ac}	230	[V]
Output ac frequency f_1	50-1k	[Hz]
Switching frequency f_s	10k-200k	[Hz]
Output power P	10	[kW]
Cell capacitor voltage V_c	350	[V]
Number of cell per arm N	2	[ ]

The most important parameters during the design of a MMC are: the number of sub-modules (SMs) per arm (N), the voltage and current ratings of power devices and the design of SM capacitors (C_{sm}) and arm inductors (L_{arm}). Moreover, the control of the MMC is also a relevant point. The main aspects to consider during the design and control of a MMC, together with a frequency influence analysis is explained in following subsections. In this analysis a scaled MVD is simulated, considering only two half-bridge SMs (see Fig. 4) per arm.

Reactive components

The sizing of C_{sm} and L_{arm} are key factors during the design of a MMC, since they largely define the weight and the size of the overall system. It is a well-known fact that the increase of operation frequency usually reduces the volume of magnetic elements, something already put into practice in low-power applications thanks to the availability of fast and efficient semiconductors. Otherwise, this fact is becoming a reality in high-power applications due to new WBG semiconductors better performance [2] and the development of new magnetic materials with higher magnetic saturation and lower loss densities [11]. The tendency of these reductions is relatively clear in some power converters with a unique operation frequency, such as dc-dc converters, but the impact of frequencies on reactive components of a MMC is not so evident, and further analysis is needed.

The capacitor of each SM (C_{sm}) must be large enough to limit the voltage ripple and satisfy the voltage requirements of all components. Considering that the sum of all cells of an arm can be modelled as an equivalent capacitor, and knowing that the arm current is sinusoidal (about the half of the output current), it can be deduced that the C_{sm} could depend on the transferred power and the fundamental frequency. The value of the minimum C_{sm} to obtain a certain voltage ripple (ΔV) can be calculated using (6) [12]:

$$C_{sm} \geq \frac{P}{3 \cdot N \cdot \Delta V \cdot V_c^2 \cdot m \cdot \omega} \cdot \sqrt{\left[1 - \left(\frac{m \cdot \cos\phi}{2}\right)^2\right]^3} \tag{6}$$

where P is the transferred power by the converter, N the number of SM per arm, V_c the capacitor mean voltage value, m the modulation index, ω the angular output frequency and ϕ the angular displacement of the load.

The L_{arm} of a MMC has three main tasks. First, it serves as a link inductor, limiting the arm current in each commutation and making possible exchanging energy between the converter and the AC system. Second, it limits the currents in case of faults. And third, it is used to reduce the circulating currents and their resonance among arms [12]. In this context, the inductor value depends on the switching frequency, and its value can be deduced with (7) [12]:

$$L_{arm} \geq \frac{V_c}{2 \cdot f_{sw} \cdot \Delta I_{diff}} \tag{7}$$

being f_{sw} the switching frequency and ΔI_{diff} the differential current ripple.

Control strategy

The MMC topology needs several control techniques in order to regulate current and voltage values within the safe operation area: current control, total voltage balancing, differential voltage balancing, differential current suppressing control and capacitor voltage balancing. Fig. 5 illustrates the main control diagram implemented in this work.

- a) Current control: A resonant-proportional (8) controller has been implemented in order to control the sinusoidal current of each output AC phase. The references of these AC currents will define the transferred power by MMC.

$$C_{PR}(s) = K_p + K_r \frac{s}{s^2 + \omega_0^2} \tag{8}$$

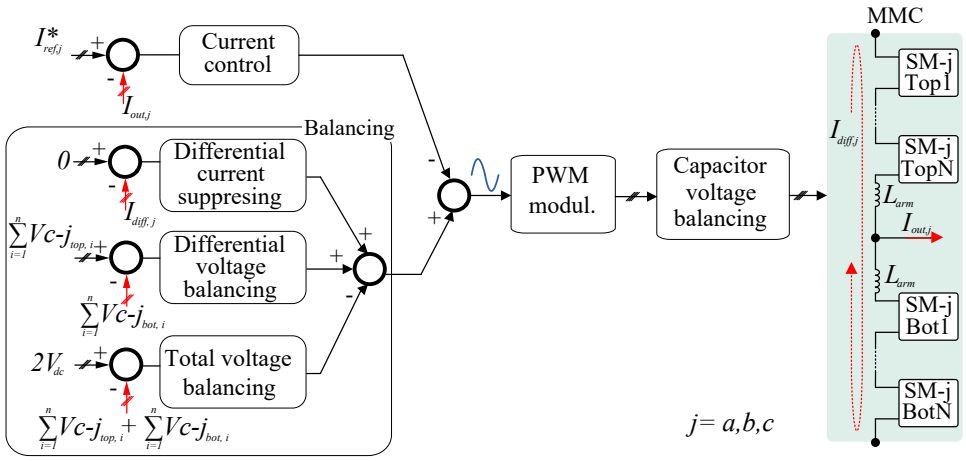

Fig. 5: Control diagram of each MMC phase.

where K_p is the Proportional Gain term, K_r is the Integral Gain term of the resonant controller and ω_0 is the resonance frequency.

- *b*) Total voltage balancing: The balancing of the total voltage or the sum of all cell capacitor voltages (and thus the balancing of total energy of each leg (j = a,b,c) can be regulated using an integral controller. This control tries to achieve the condition (9).

$$\sum_{i=1}^{N} V_{c-j,top\,i} + \sum_{i=1}^{N} V_{c-j,bot\,i} = 2V_{dc} \tag{9}$$

where $V_{c-j,top\,i}$ is the capacitor voltage of each SM from the top arm, $V_{c-j,bot\,i}$ is related to the bottom ones and V_{dc} is the HVDC input voltage.

- *c*) Differential voltage balancing: The balancing of differential energy of arms is achieved using another integral controller. The objective of this control is to equalize the sum of the capacitor voltage of top and bottom arms (10).

$$\sum_{i=1}^{N} V_{c-j,top\,i} = \sum_{i=1}^{N} V_{c-j,bot\,i} \tag{10}$$

- *d*) Differential current suppressing: An additional control is included in this work using [13] in order to reduce the differential current $I_{diff,j}$.
- *f*) Capacitor voltage balancing: Finally, the modulation strategy has also some degrees of freedom, which are used to implement an algorithm to balance the capacitor voltages of each arm, ensuring the right voltage level in all the MMC capacitors.

Frequency influence analysis

The proposed MVD converter has been simulated using PLECS, to show the influence of the switching and fundamental frequencies on the design of reactive components. Fig. 6 shows the differential current of each leg ($I_{diff,j}$) together with the amount of SM voltages ($V_{c,j}$) for different frequency combinations. According to these simulation results, the impact of the fundamental frequency only affects to the capacitor, and it is inversely proportional to the required capacitive value. Moreover, simulation results illustrate that the inductor current ripple (ΔI_{diff}) depends on the switching frequency. The most critical feature to select the inductance value is the resonance circulating current [12]. However, using circulating current suppression control [13], the critical factor of the arm inductor value becomes the switching frequency.

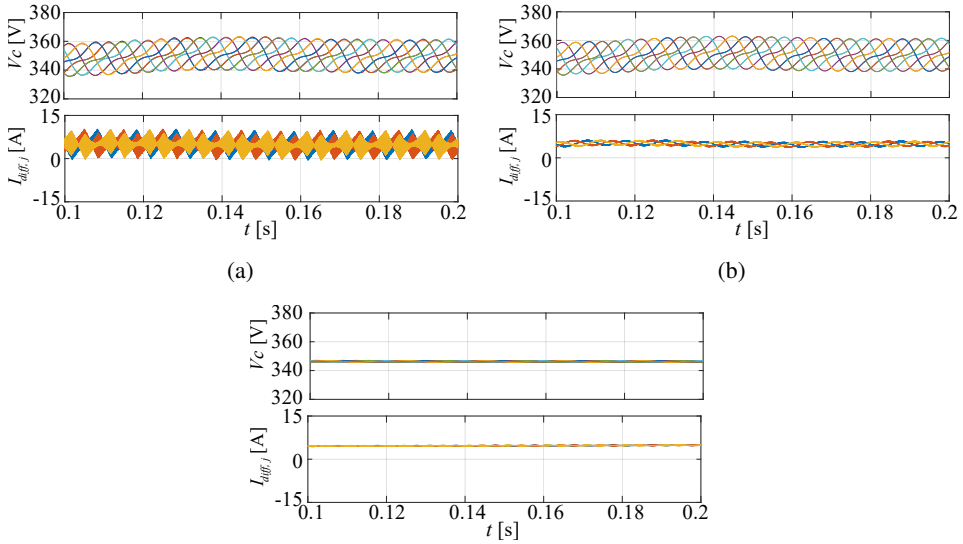

Fig. 6: Fundamental and switching frequency impact on reactive components of the proposed MMC. MVD SMs voltage ($V_{c,j}$) and three-phase differential current $I_{diff,j}$ for different frequencies: (a) $f_1 = 50\,Hz$, $f_{sw} = 10\,kHz$, (b) $f_1 = 50\,Hz$, $f_{sw} = 200\,kHz$ and (c) $f_1 = 1\,kHz$, $f_{sw} = 200\,kHz$.

MMC performance evaluation

Once the effect of system frequencies is analysed, the performance of GaN HEMT and Si CoolMOS based MMC are compared, evaluating the distribution of power losses. In this case, a commercial air forced cooling system is defined with a 3.5 K/W heatsink-to-ambient resistance ($R_{th_{ha}}$) and a thermal interface material (TIM) of 2.25 K/W. This cooling system determines the power loss limit (P_{limit}) of the SM around 20 W for each semiconductor technology, with a maximum junction temperature (T_j) of 150 °C. The driving and switching losses of power devices are obtained by the product of energies and switching frequency. GaN device has lower driving losses than Si device due to lower Q_G and lower driving voltage (1). That is an important factor due to the number of devices used for the MMC topology ($4 \cdot N \cdot N_{ph}$ with half-bridge SM). In this case, as the MVD is scaled down (N=2 / N_{ph}=3), the impact of driving losses is not that high, as it is shown in Table III. However, the use of GaN devices reduces greatly driving losses and it will be an important factor to MMCs with large number of SMs.

Table III: MMC SM driver loss comparison.

	10 kHz			200 kHz			Unit
	per switch	per SM	TOTAL	per switch	per SM	TOTAL	
Si CoolMOS	6.8	13.6	163.20	136	272	3264	[mW]
GaN HEMT	0.38	0.75	9.05	7.54	15.08	180.96	[mW]

Regarding conduction and switching losses, distribution of power losses is modelled in PLECS, comparing the results obtained by GaN and Si devices for different fundamental and switching frequencies. The power loss distribution for a balanced MMC is the same for every SM, as can be deduced from Fig. 7. Although conduction losses (P_{cond}) are the most relevant power losses factor for common 'low-frequency' MMCs (Fig. 7(a)), the higher the switching frequency is, the lower is the impact of conduction losses on overall system performance. Moreover, GaN-based MMC has lower losses than the one based on Si devices for high-switching frequency, as a result of lower turn-on switching losses ($P_{on_i} + P_{on_{rr}}$). Otherwise, the fundamental frequency does not affect to power losses of devices, as can be deduced comparing Fig. 7(b) to Fig. 7(c).

It is worth noting that it is not possible to use Si devices for high-switching frequency (200 kHz) due to

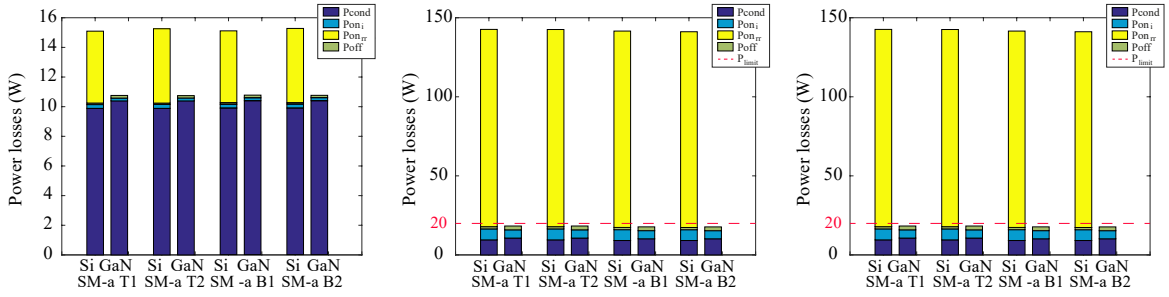

Fig. 7: Power loss distribution analysis of GaN HEMT and Si CoolMOS based MMC leg. Conduction losses (P_{cond}), turn-on losses (without recovery energy) (P_{on_i}), reverse recovery turn-on losses ($P_{on_{rr}}$) and turn-off losses (P_{off}) for different frequencies: (a) $f_1 = 50\,Hz$, $f_{sw} = 10\,kHz$, (b) $f_1 = 50\,Hz$, $f_{sw} = 200\,kHz$ and (c) $f_1 = 1\,kHz$, $f_{sw} = 200\,kHz$.

the great impact of reverse recovery power losses ($P_{on_{rr}}$), overcoming the power loss limit (P_{limit}) of the cooling system.

Experimental validation

The distribution of power losses for GaN devices is validated by experimental measurements. For that purpose, a commercial GaN-based evaluation board is used, which is based on same GaN power devices presented in Table I. This evaluation board contains two GaN HEMT on half-bridge configuration, as the SM of the analysed MMC. An experimental analysis of power losses is performed under different operation conditions. Converter power loss values at different switching frequencies are obtained to separate conduction and switching losses.

Fig. 8 shows that the power losses of GaN devices are well estimated, in spite of the mismatch between the analytical calculation and experimental results, considering the amount of factors that are not taken into account which affect to the difference (e.g. junction temperature difference, PCB stray inductance, measurement accuracy...). However, even if the obtained power losses are low, it is mandatory to perform an exhaustive thermal analysis in order to extract the heat from such small devices.

Considering these results, a GaN based MMC prototype is developed with higher current capability GaN devices and ensuring a better thermal performance. Fig. 9 shows one of the developed SM with some preliminary temporal measurements. The full GaN-based MMC will be analysed and presented in future works.

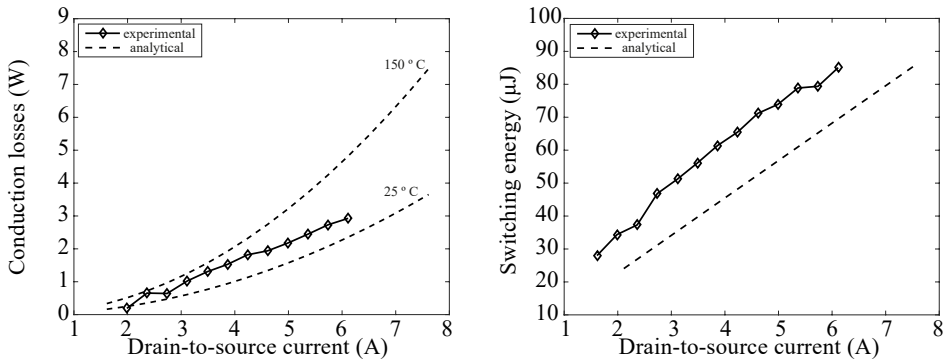

Fig. 8: Experimental validation of analytical GaN HEMT power loss characteristics (V_{in} = 350 V): (a) Conduction losses and (b) Switching losses ($E_{ON} + E_{OFF}$).

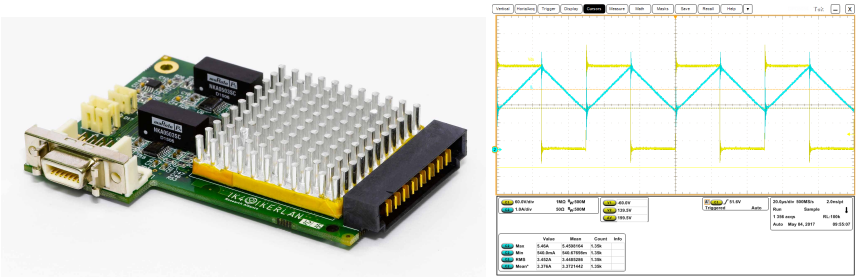

(a) (b)

Fig. 9: The SM of the developed GaN-based MMC prototype (a) and preliminary experimental measurements (b).

Conclusions

This paper presents a performance evaluation of a MMC based on Si CoolMOS and GaN HEMT power devices. The influence of the MMC operation frequencies and the power loss distribution have been analysed using analytical estimations and PLECS simulation tool. The increase of switching and fundamental frequencies results in a reduction of differential current and capacitance voltage, respectively. Furthermore, GaN device is presented as a proper solution for high-switching MMC converter due to its better turn-on switching losses and lower gate requirements comparing with its Si counterparts. However, Si CoolMOS will be a suitable solution for lower switching frequencies, where the conduction losses has the greatest impact. A GaN-based MMC converter is developed considering the low power loss performance of GaN devices and the reduction of the converter size due to high-switching operation.

References

[1] A. Mantooth, "Devices and Components for New Power Converter Developments," *IEE Power Electronics Magazine*, no. 6, pp. 53–56, June 2016.

[2] J. Millan, P. Godignon, X. Perpina, A. Perez-Tomas, and J. Rebollo, "A Survey of Wide Bandgap Power Semiconductor Devices," *IEEE Transactions on Power Electronics*, vol. 29, no. 5, pp. 2155–2163, May 2014.

[3] J. Dorn, H. Gambach, J. Strauss, T. Westerweller, and J. Alligan, "Trans Bay Cable – A Breakthrough of VSC Multilevel Converters in HVDC Transmission," in *CIGRE San Francisco Colloq.*, 2012.

[4] M. a. Perez, D. Arancibia, S. Kouro, and J. Rodriguez, "Modular Multilevel Converter with Integrated Storage for Solar Photovoltaic Applications," in *Industrial Electronics Society (IECON)*, 2013.

[5] SIEMENS, "Sinamics sm120." [Online]. Available: http://www.industry.siemens.com/drives/global/en/converter/mv-drives/pages/sinamics-sm120-cm.aspx

[6] A. Lesnicar and R. Marquardt, "An Innovative Modular Multilevel Converter Topology Suitable for a Wide Power Range," in *PowerTech Conference*, 2003.

[7] D. Peftitsis, G. Tolstoy, and A. Antonopoulos, "High-Power Modular Multilevel Converters with SiC JFETs," *IEEE Transactions on Power Electronics*, vol. 27, no. 1, pp. 28–36, Jan. 2012.

[8] D. Graovac, M. Pürschel, and K. Andreas, "Application Note: MOSFET Power Losses Calculation Using the Data- Sheet Parameters," 2006. [Online]. Available: http://application-notes.digchip.com/070/70-41484.pdf

[9] Semikron, "Application Manual Power Semiconductors," 2015. [Online]. Available: https://www.semikron.com/dl/service-support/downloads/download/semikron-application-manual-power-semiconductors-english-en-2015

[10] M. A. Perez, S. Bernet, J. Rodriguez, S. Kouro, and R. Lizana, "Circuit Topologies, Modelling, Control Schemes and Applications of Modular Multilevel Converters," *IEEE Transactions on Power Electronics*, vol. 30, no. 1, pp. 4–17, Jan. 2015.

[11] A. Krings, A. Boglietti, A. Cavagnino, and S. Sprague, "Soft Magnetic Material Status and Trends in Electric Machines," *IEEE Transactions on Industrial Electronics*, vol. 64, no. 3, pp. 2405 – 2414, Mar. 2016.

[12] Z. Xu, H. Xiao, and Z. Zhang, "Selection methods of main circuit parameters for modular multilevel converters," *IET Renewable Power Generation*, vol. 10, no. 6, pp. 788–797, Jun. 2016.

[13] Q. Tu, S. Member, Z. Xu, L. Xu, and S. Member, "Reduced Switching-Frequency Modulation and Circulating Current Suppression for Modular Multilevel Converters," *IEEE Transactions on Power Delivery*, vol. 26, no. 3, pp. 2009–2017, Mar. 2011.